Article:
Cook, J.M., Tedstone, A.J., Williamson, C. et al. (21 more authors) (2020) Glacier algae accelerate melt rates on the south-western Greenland Ice Sheet. The Cryosphere, 14 (1). pp. 309-330. ISSN 1994-0416

https://doi.org/10.5194/tc-14-309-2020

Supplement of The Cryosphere, 14, 309–330, 2020
https://doi.org/10.5194/tc-14-309-2020-supplement

The Cryosphere Open Access EGU

Supplement of

Glacier algae accelerate melt rates on the south-western Greenland Ice Sheet

Joseph M. Cook et al.

Correspondence to: Joseph M. Cook (joc102@aber.ac.uk)

Cook et al. 2019: Glacier algae accelerate melting of the south-western Greenland Ice Sheet, The Cryosphere.

S1:

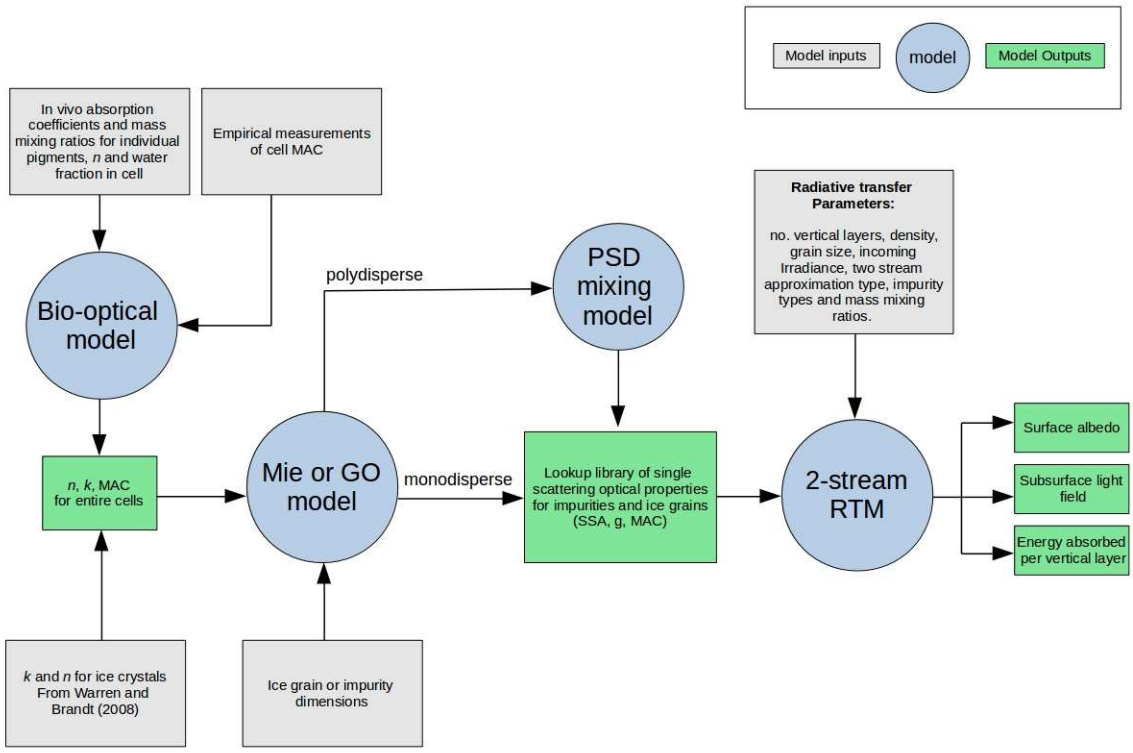

Schematic showing the structure of the BioSNICAR_GO radiative transfer package

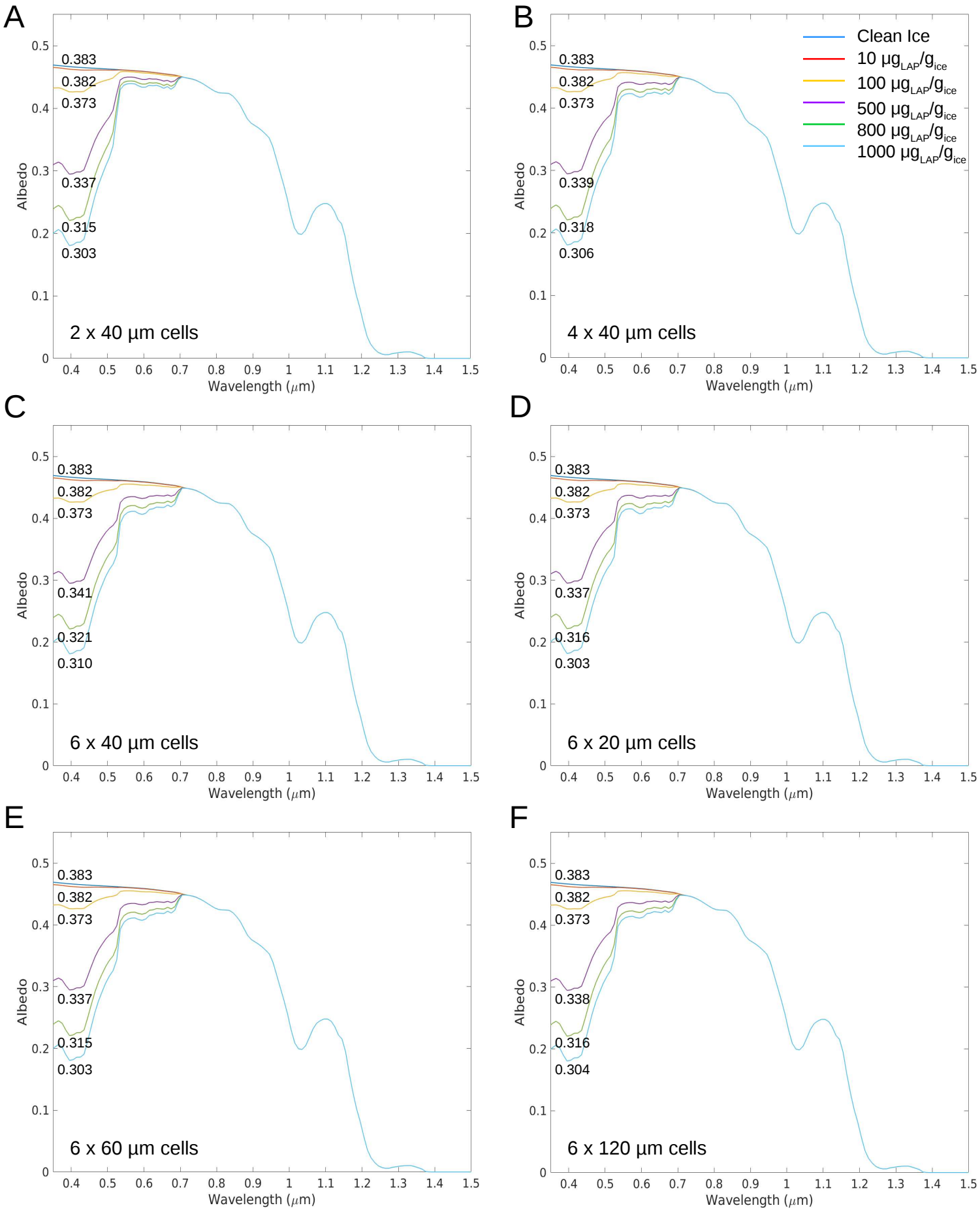

S2: Simulated albedo with 10 – 1000 µg/g algae of varying cell size. Broadband albedo is printed beneath each curve.

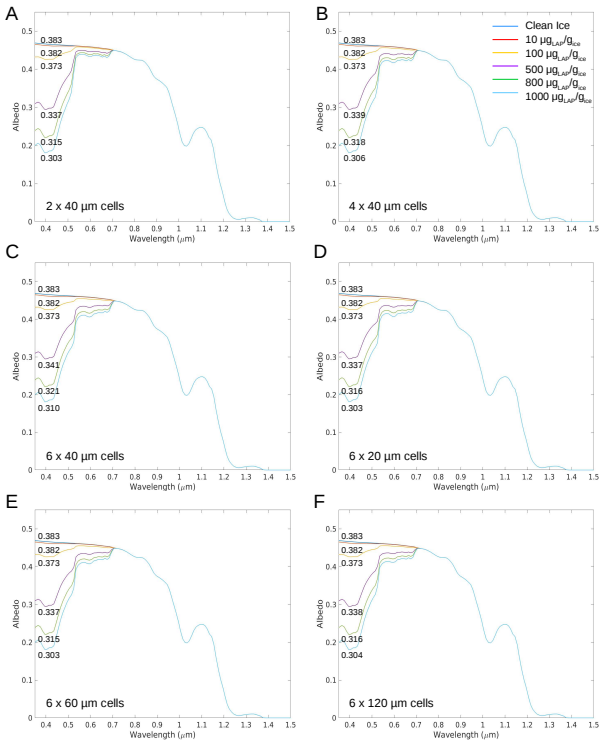

S2: Simulated albedo with 10 – 1000 μg/g algae of varying cell size. Broadband albedo is printed beneath each curve.

Cook et al. 2019: Glacier algae accelerate melting of the south-western Greenland Ice Sheet, The Cryosphere.

S3: Mineral dust sampling and particle size distribution (PSD).

High algal biomass ice samples were collected in sterile sample bags and melted at ambient temperatures (5-10 °C). The thawed samples were filtered onto glass fiber filters (0.7 µm pore size), from which the solids were removed into a glass jar using a stainless steel spatula. In 50 mL centrifuge tubes, the samples were treated using 30% H_2O_2 (w/w) (Honeywell Fluka™) to remove the organic fraction. The samples (1-2 g) were sonicated (VWR ultrasonic cleaner) in 45 mL of the H_2O_2 treatment for 10 min to disaggregate the material. The samples were left in the H_2O_2 treatment for 48 h, after which they were centrifuged for 10 min at 4000 rpm (Eppendorf centrifuge 5810). The supernatant was removed, and the H_2O_2 solution was replaced. This process was repeated up to ten times until no more organic oxidation was observed. The remaining mineral fraction was washed three times in water (Sartorius arium® pro ultrapure water), with centrifugation after each wash.

A 5 mg of H_2O_2-treated sample was suspended in 10 mL of ultrapure water. The sample was sonicated to disaggregate the grains. The suspension was dispersed onto a 0.2 µm polycarbonate filter (Sartorius Track-Etch Membrane, 0.2 µm). Once dry, a section of each filter was adhered to a stainless steel SEM stub using an adhesive carbon tab. The sample was coated with 8 nm of Ir (Agar high resolution sputter coater). The PSD was determined using a Zeiss Ultra Plus field emission scanning electron microscope (FE-SEM) operated at 20 kV. Automated particle counting software was used to determine the PSD in an area of approximately 1 mm^2.

Cook et al. 2019: Glacier algae accelerate melting of the south-western Greenland Ice Sheet, The Cryosphere.

S4:

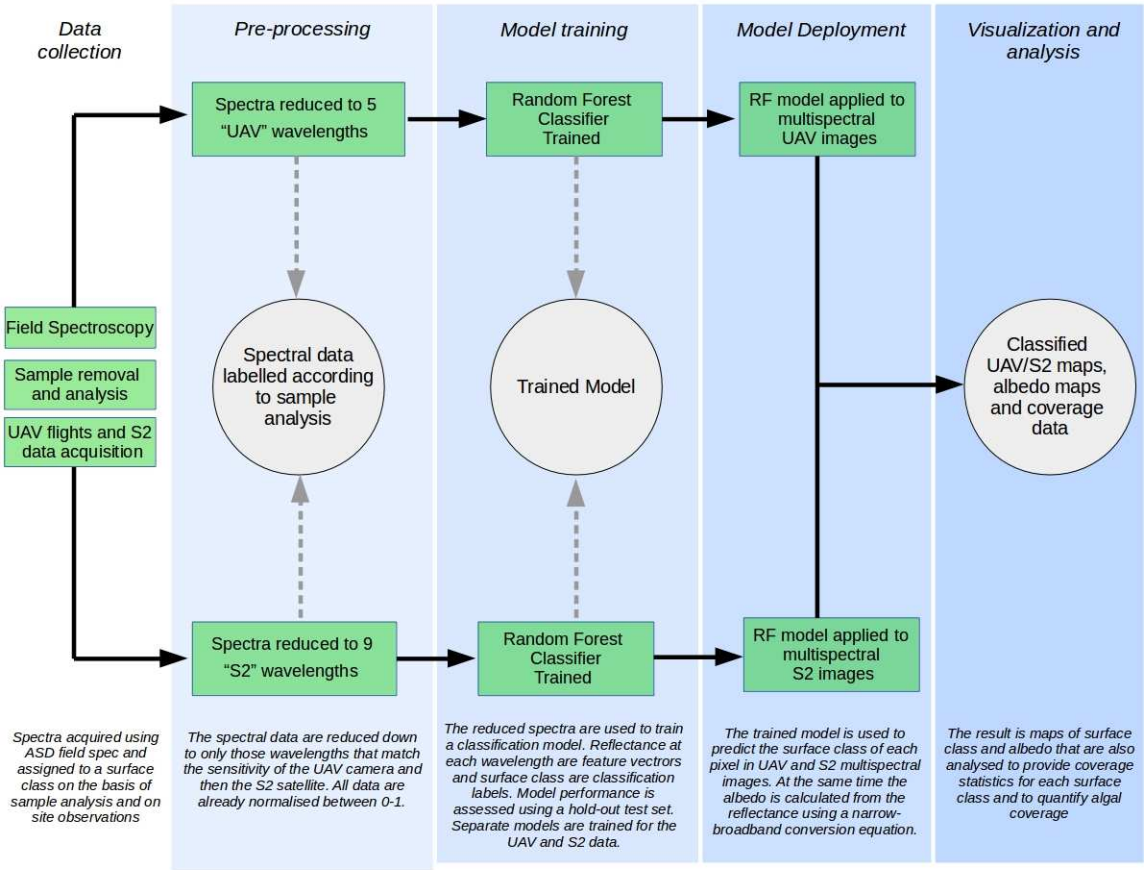

Schematic showing the remote sensing classification workflow.

Cook et al. 2019: Glacier algae accelerate melting of the south-western Greenland Ice Sheet, The Cryosphere.

S5:

A:

Model	Accuracy	Precision	Recall	F1 Score
K-Nearest Neighbours	0.90	0.74	0.78	0.76
Naive-bayes	0.90	0.80	0.81	0.80
Support Vector Machine	0.94	0.89	0.87	0.88
Random Forest	0.99	0.99	0.95	0.97
Ensemble	0.92	0.76	0.81	0.78
RF performance on test set	**0.90**	**0.91**	**0.90**	**0.90**

B:

Model	Accuracy	Precision	Recall	F1 Score
K-Nearest Neighbours	0.89	0.90	0.89	0.87
Naive-bayes	0.89	0.89	0.89	0.89
Support Vector Machine	0.96	0.96	0.96	0.96
Random Forest	0.99	0.99	0.99	0.99
Ensemble	0.93	0.93	0.93	0.93
RF performance on test set	**0.92**	**0.93**	**0.92**	**0.93**

Table 1: A) Performance metrics for supervised classification algorithms on training data using five bands coincident with MicaSense Red-Edge multispectral imagery, plus the final model performance on the test set; B) Performance metrics for supervised classification algorithms on training data using eight bands coincident with Sentinel-2 multispectral imagery, plus the final model performance on the test set.

Cook et al. 2019: Glacier algae accelerate melting of the south-western Greenland Ice Sheet, The Cryosphere.

S6:

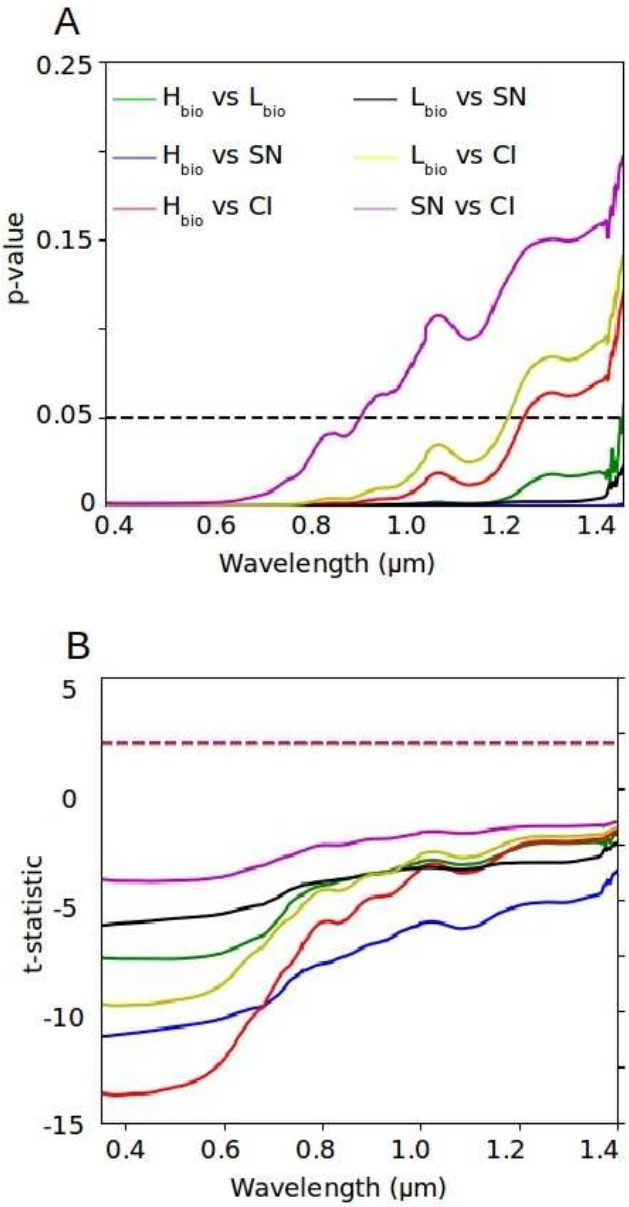

Cook et al. (2019), Glacier algae accelerate melt rates on the south-western Greenland Ice Sheet. The Cryosphere.

S7:

In this supplementary information we describe additional radiative transfer experiments that tested the sensitivity of ice albedo to different types of dust. In all cases, the simulations were run with diffuse illumination, ice crystal side-length and diameter per vertical layer = 3, 4, 5, 8, 10 mm, layer thicknesses = 0.1, 1, 1, 1, 1 cm, underlying surface albedo = 0.15, layer densities = 500, 500, 600, 600, 600 kg m^{-3}. These ice physical properties were chosen to reduce the absolute error between the simulated albedo for ice without any impurities ('clean ice') and our mean field-measured clean-ice spectrum and match those used for the simulations reported in the main manuscript.

We incorporated optical properties for bulk minerals from Flanner et al. (2009) and Polashenski et al. (2015) into our radiative transfer model to test the sensitivity of the ice albedo to dusts with smaller PSD and greater abundance of darker minerals, in particular iron-rich hematite that was assumed to be the main light-absorbing particle in dust samples from Greenland snow (Polashenski et al. 2015). The dusts from Polashenski et al. (2015) represent three scenarios with low (2.7 %), median (5.6 %) and high (9.3 %) hematite, with the non-hematite component comprising illite, montmorillonite, calcite, kaolinite, anthropogenic particulates and quartz. The bulk samples each had a lognormal PSD with volume-mode radii ranging from 0.8 um (assumed in the high scenario) to 2.0 um (assumed in the low scenario). We refer to these samples as P1, P2 and P3 for low, median and high hematite respectively. Four "global average" dusts from Flanner et al. (2009), which have typical Saharan optical properties, were included and referred to as F1, F2, F3 and F4. The mineralogy of each of these dusts are identical but the grain radii differ (F1 = 0.05 – 0.5 μm; F2 = 0.5 – 1.25 μm; F3 = 1.25 – 2.5 μm; F4 = 2.5 – 5.0 μm). We highlight that none of these "F" or "P" dusts are considered to be realistic for our field site, but are included in order to test the robustness of the ice albedo to different mineral mixtures, in particular in cases where strongly absorbing red-coloured minerals comprise a greater fraction of the bulk mineralogy relative to our field samples.

The Saharan-type dusts F1 and F2, which have the smallest size distributions, caused the broadband albedo of the ice to increase, with a greater increase at larger mass mixing ratios, caused by the reduction in albedo at shorter visible wavelengths being exceeded by albedo increases at longer NIR wavelengths. This is the result of the large ice-grain sizes used in the simulations. When we repeated the simulations using snow grains (with optical properties calculated using Mie theory) 1000 $\mu g_{dust}/g_{ice}$ of the F1 dusts had an albedo-lowering effect of 0.016 for grain radii of 1000 μm. For 1000 $\mu g_{dust}/g_{ice}$ of the F2 dusts the albedo reduction was 0.026.

At our mean measured mineral mass-mixing ratio (342 $\mu g_{dust}/g_{ice}$) the Saharan-type dusts (F3 and F4) had a larger albedo reducing effect than the local dusts, with F3 reducing the albedo by 0.003 and F4 reducing the albedo by 0.005, compared to 0.002 for MN-DUST (Table S8.1, Fig S8.1). For P1 – P3 the same mass-mixing ratio reduced the albedo by 0.0002, 0.004 an 0.014. For dusts P1-P3 some but not all of the albedo reduction in the visible wavelengths is offset by increases in the NIR wavelengths. For comparison, glacier algae at the mean measured mass-mixing ratio reduced the albedo by 0.04. The albedo reduction caused by glacier algae exceeds that of the mineral dusts by at least an order of magnitude except in the case of the high-hematite P3, in which case the albedo-reducing effect of glacier algae was greater by a factor of 2.8 at the mean measured mass-mixing ratio and 2.7 at the maximum measured mass-mixing ratio (646 $\mu g_{dust}/g_{ice}$).

Despite their small effect on broadband albedo, hematite-rich dusts P1-3 did reduce the albedo across the visible wavelengths. The phenomenon of visible-wavelength albedo-lowering being offsett by increased NIR albedo is exacerbated by the very large grain sizes in our study. This indicates that in areas where hematite-rich dusts are prevalent they may have an appreciable albedo-lowering effect if the ice grain size is smaller. They may also create ambiguity in remote detection of algae where the spectral resolution of the sensor is low.

It is also informative to examine spectral features in the algal- and mineral-influenced albedo. The spectral shape produced by glacier algae differs from that of any of the mineral dusts. For the local dusts (HI-DUST, LO-DUST, MN-DUST) the shape of the clean-ice spectrum is only slightly modified by their addition at the

mass mixing ratios included in our study, creating no specific spectral features. For the Saharan-type (F1-F4) and hematite-rich dusts (P1-P3) the ice albedo is depressed preferentially at short visible wavelengths, increasing with wavelength up to 0.70 μm. For glacier algae, the spectrum is much flatter between 0.40 and 0.45 μm before rising steeply to the “chlorophyll-a bump” at 0.55 μm, gently rising to the chlorophyll absorption feature at 0.68 μm and increasing steeply at the “red-edge” to 0.70 μm. In general, these spectral features are consistent with our field spectra for algal ice, although we point out that our field spectra are modified by additional feedbacks, for example to grain size and shape, that are not accounted for in the model. These spectral features may enable remote detection of glacier algae and separation of spectral signatures for surfaces containing both glacier algae and red dust in areas where this is necessary, providing the sensor has sufficient spectral resolution.

References:

Flanner, M.G., Zender, C.S., Hessm P.G., Mahowald, N.M., Painter, T.H., Ramanathan, V., Rasch, P.J., Springtime warming and reduced snow cover from carbonaceous particles. Atmospheric Chemistry and Physics, 9: 2481-2497, 2009.

Polashenski, C. M., Dibb, J. E., Flanner, M. G., Chen, J. Y., Courville, Z. R., Lai, A. M., Schauer, J. J., Shafer, M. M., Bergin, M. Neither dust nor black carbon causing apparent albedo decline in Greenland's dry snow zone: Implications for MODIS C5 surface reflectance, *Geophys. Res. Lett.*, 42, 9319– 9327, doi:10.1002/2015GL065912, 2015.

	Albedo change for various light absorbing impurity mass mixing ratios								
	Hypothetical mass mixing ratios ($\mu g_{LAP}/g_{ice}$)					**Measured mass mixing ratios ($\mu g_{LAP}/g_{ice}$)**			
	10	**100**	**500**	**800**	**1000**	**342**	**349**	**519**	**646**
Glacier algae	-0.0010	-0.0110	-0.0460	-0.0670	-0.0800	-0.0300	-0.0400	-0.0487	-0.0560
HI-DUST	-0.0001	-0.0006	-0.0030	-0.0048	-0.0060	-0.0021	-0.0023	-0.0033	-0.0039
LO-DUST	-0.0001	-0.0004	-0.0021	-0.0034	-0.0042	-0.0015	-0.0016	-0.0023	-0.0028
MN-DUST	<0.0001	<0.0001	-0.0020	-0.0043	-0.005	-0.0010	-0.0020	-0.0029	-0.0035
F1	0.0006	0.0061	0.0285	0.0435	0.0528	0.0200	0.0221	0.0305	0.0360
F2	0.0001	0.0014	0.0066	0.0103	0.0126	0.0046	0.0051	0.0071	0.0084
F3	-0.0001	-0.0009	-0.0042	-0.0066	-0.0081	-0.0029	-0.0032	-0.0045	-0.0053
F4	-0.0001	-0.0014	-0.0066	-0.0105	-0.0130	-0.0046	-0.0051	-0.0071	-0.0085
P1	<0.0001	<0.0001	<0.0001	0.0003	0.0007	-0.0002	-0.0002	<0.0001	0.0000
P2	-0.0002	-0.0015	-0.0050	-0.0057	-0.0055	-0.0040	-0.0043	-0.0052	-0.0055
P3	-0.0005	-0.0050	-0.0182	-0.0228	-0.0240	-0.0141	-0.0152	-0.0190	-0.0209

Table S6.1: Albedo change (4 d.p.) relative to clean ice caused by the addition of each LAP to the upper 1 mm of ice in a range of mass mixing ratios from 10 to 1000 $\mu g_{LAP}/g_{ice}$.

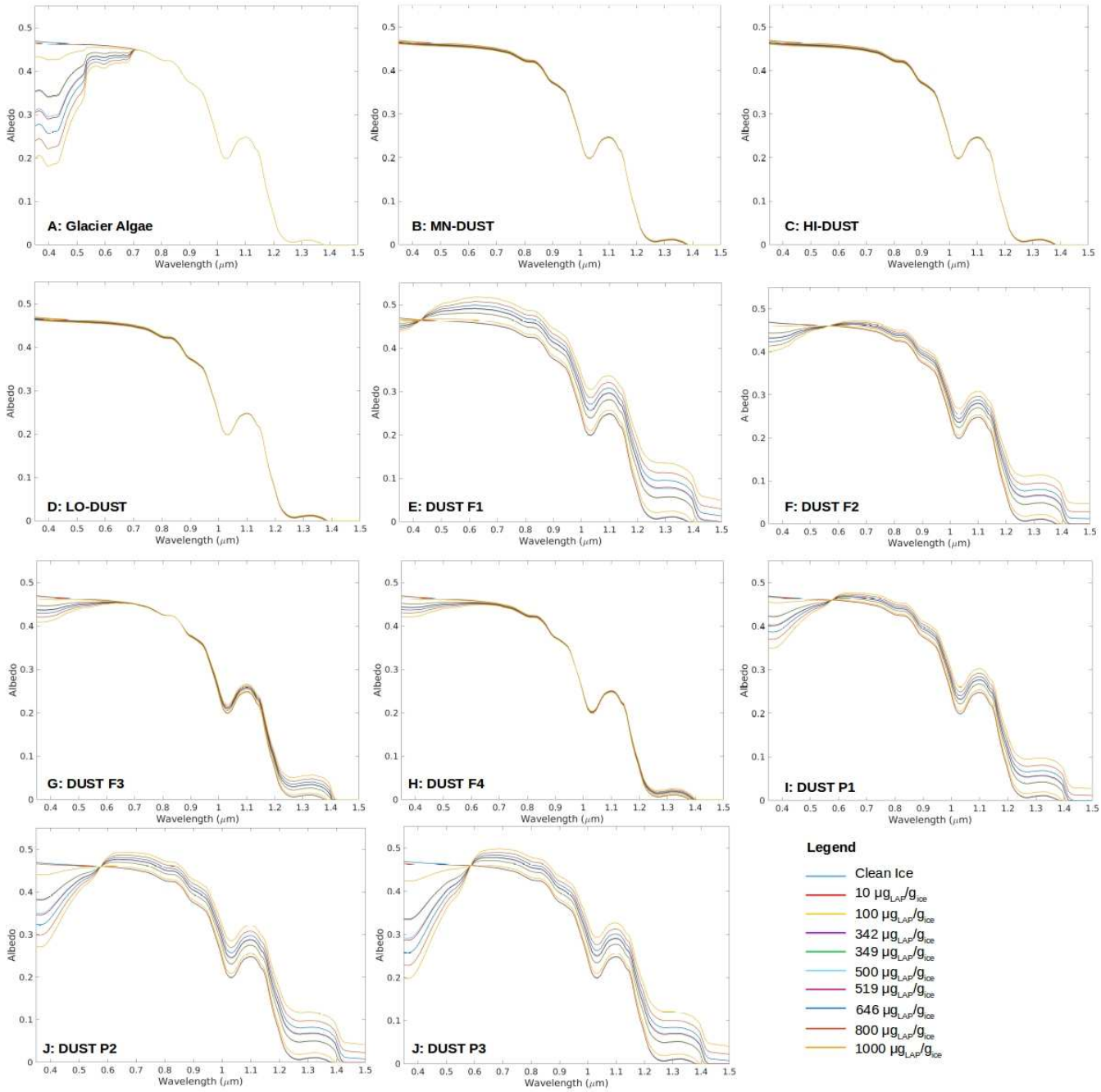

Fig S7.1: Spectral albedo for each of our sensitivity tests.

Cook et al. 2019: Glacier algae accelerate melting of the south-western Greenland Ice Sheet, The Cryosphere.

S8: